ADVANCED FUNCTIONAL MATERIALS

Photocrosslinkable Polythiophenes for Efficient, Thermally Stable, Organic Photovoltaics

By *Bumjoon J. Kim, Yoshikazu Miyamoto, Biwu Ma,* and *Jean M. J. Fréchet**

Photocrosslinkable bromine-functionalized poly(3-hexylthiophene) (P3HT-Br) copolymers designed for application in solution-processed organic photovoltaics are prepared by copolymerization of 2-bromo-3-(6-bromohexyl) thiophene and 2-bromo-3-hexylthiophene. The monomer ratio is carefully controlled to achieve a UV photocrosslinkable layer while retaining the π–π stacking feature of the conjugated polymers. The new materials are used as electron donors in both bulk heterojunction (BHJ) and bilayer type photovoltaic devices. Unlike devices prepared from either P3HT:PCBM blend or P3HT-Br:PCBM blend without UV treatment, photocrosslinked P3HT-Br:PCBM devices are stable even when annealed for two days at the elevated temperature of 150 °C as the nanophase separated morphology of the bulk heterojunction is stabilized as confirmed by optical microscopy and grazing incidence wide angle X-ray scattering (GIWAXS). When applied to solution-processed bilayer devices, the photocrosslinkable materials show high power conversion efficiencies (∼2%) and excellent thermal stability (3 days at 150 °C). Such performance, one of the highest obtained for a bilayer device fabricated by solution processing, is achieved as crosslinking does not disturb the π–π stacking of the polymer as confirmed by GIWAXS measurements. These novel photocrosslinkable materials provide ready access to efficient bilayer devices thus enabling the fundamental study of photophysical characteristics, charge generation, and transport across a well-defined interface.

1. Introduction

Polymer based organic photovoltaics have attracted a great deal of attention due to the potential cost-effectiveness of light-weight and flexible solar cells.[1–5] A significant breakthrough was achieved with the advent of bulk-heterojunction (BHJ) devices based on π-conjugated polymers as electron donors and fullerene derivatives as electron acceptors.[6–11] Although a number of polymer–fullerene combinations have been tested,[11–13] BHJ solar cells based on poly(3-hexylthiophene) (P3HT) and the fullerene derivative [6,6]-phenyl-C_{61}-butyric acid methyl ester (PCBM) still represents the state of the art in organic photovoltaics with reproducible efficiencies as high as 5%.[9,10,14–16]

A key parameter for efficient BHJ solar cells is the three-dimensional nanomorphology of the active layer that provides a large interfacial area for exciton dissociation.[17,18] The size of the electron donor and electron acceptor domains should be targeted such that the phase separation lengthscale is comparable to that of the exciton diffusion length (∼5 nm)[19,20] while maintaining the co-continuous pathway for charge transport to the electrodes. Although the active layer of BHJ solar cells can be easily produced by spin casting a blend solution on substrates, the control of donor–acceptor blend morphology is extremely difficult since the morphology is obtained by kinetically trapping a non-equilibrium state during the process of spinodal decomposition. Most BHJ polymer solar cells are not thermally stable as subsequent exposure to heat drives further development of the morphology towards a state of macrophase separation in the micrometer scale.[3,5] Improving the thermal stability of BHJ solar cells is important for the future application of these devices since any heat generated by solar irradiation could be detrimental to the performance of these devices as a result of the relatively low T_g of polymers and the strong immiscibility of components in the active layer.

Two major routes have been reported to improve the thermal stability of conjugated polymer-fullerene BHJ photovoltaic devices. One involves the use of compatibilizers having two different blocks of conjugated polymers and fullerenes to act as a compatibilizer reducing the interfacial tension between the two dissimilar components of the BHJ thus retarding their phase separation.[21] However, the synthesis of compatibilizers is not trivial due to the multiple post-polymerization steps and the low solubility of fullerenes. The other approach explored the use of thermally crosslinkable units such as an epoxide-functionalized PCBM as a means to prevent phase segregation on one of the materials. Unfortunately, the crosslinking led to significantly

[*] Prof. J. M. J. Fréchet, Dr. B. J. Kim, Y. Miyamoto, Dr. B. Ma
Materials Science Division
Lawrence Berkeley National Laboratory and Department of Chemistry
University of California
Berkeley, CA 94720-1460 (USA)
E-mail: frechet@berkeley.edu
Dr. B. J. Kim
Department of Chemical and Biomolecular Engineering
Korea Advanced Institute of Science and Technology
Daejeon 305-701 (Korea)

DOI: 10.1002/adfm.200900043

reduced device performance in spite of the stabilized P3HT/PCBM morphology.[22,23]

The introduction of crosslinking bridges in conjugated polymers can disturb their π–π stacking, which is critical for both charge transport and light absorption.[24] More importantly, while thermal annealing is required to develop the crystalline structure of conjugated polymers and optimize BHJ morphology,[5,10] it can simultaneously activate the crosslinkers to prevent the development of such desired morphology. Therefore, although the crosslinking concept is simple and powerful, the development of materials with both stable morphology and high performance remains a challenge. The materials should be designed to match the following requirements. First, the crosslinkers should not be activated by thermal annealing so that the morphology development can be optimized separately. Second, the crosslinking units should be small in size and efficient enough to freeze the BHJ morphology at a low concentration. This will minimize the disturbance to the π stacking of the conjugated polymers thus maintaining high charge mobility and light absorption. Finally, the crosslinkable units should be easy both to prepare and to activate.

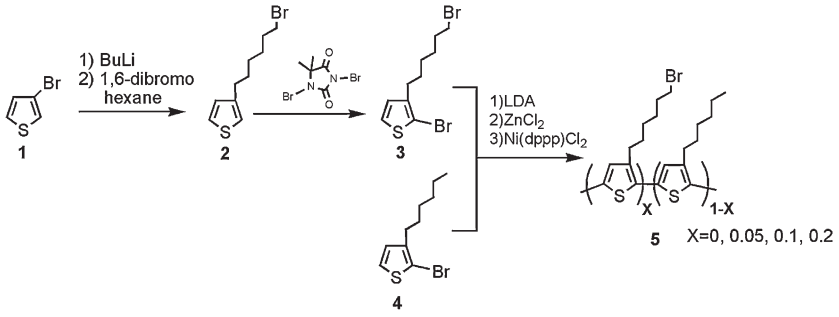

Scheme 1. Synthesis of bromine-functionalized P3HT copolymers.

This crosslinking strategy is also extremely useful for the preparation of solution processed bilayer structured devices. Despite their inherently lower efficiencies compared to that of BHJ devices, bilayer type solar cells[25–31] provide a unique platform to study the physical fundamentals of photovoltaic devices and test the relative performance of new materials. To date, efficient bilayer devices have been achieved mainly by vapor deposition of small molecules. Solution processing of bilayer structures is not trivial, as the solvent applied for the deposition of a second layer frequently dissolves or otherwise affects the previously deposited layer. In particular, it is important to minimize any disturbance in the packing of the conjugated polymer near the interface as the efficiency of a bilayer structure device is acutely affected by the short diffusion length of excitons.

Here, we have developed novel photocrosslinkable materials, bromine-functionalized poly(3-hexylthiophene) copolymers (P3HT-Br), to stabilize the BHJ film morphology with minimal disturbance in the packing of conjugated polymers, thus enabling high performing and thermally stable bilayer as well as BHJ photovoltaics.

2. Results and Discussion

2.1. Synthesis and Photocrosslinking Behavior of the New Materials

We have designed and prepared a series of bromine-functionalized poly(3-hexylthiophenes) copolymers (P3HT-Br) containing various amounts of the crosslinkable brominated unit **3** (Scheme 1). Previous work[32,33] has shown that any change in the alkyl chain of the poly(alkylthiophene) (i.e. change in alkyl chain length or modification of the end group) can affect the semicrystalline nature of the conjugated polymer leading to a significant decrease in device performance. Therefore, we have carefully chosen a small size Br substituent tethered to the end of a hexyl chain to minimize the disturbance to the packing of the P3HT polymers. 3-bromohexylthiophene (**2**) was prepared from 3-bromothiophene (**1**) by reacting with n-BuLi and 1,6-dibromohexane according to the route reported by Stokes et al.[34] 1,3-dibromo-5,5-dimethylhydantoin was then added to **2** affording photocrosslinkable monomer **3**, 2-bromo-3-(6-bromohexyl)-thiophene. The P3HT-Br copolymers **5** were synthesized by the McCullough method[35] to produce highly regioregular polymers containing various proportions of the two monomers **3** and **4** (Table 1). The polymerization mixture was quenched with 1N HCl to prevent dimerization, thus producing P3HT-Br copolymers with narrow molecular polydispersities (PDI) and the copolymers were isolated by neutralization-precipitation into methanol mixed with 7N ammonia.

The feed ratio of the two different monomers **3** and **4** was varied to produce P3HT-Br copolymers having approximately 5, 10, and 20 mol% of Br-units derived from **3**. The actual mole fraction of **3** in the copolymers was measured via ^{1}H-NMR while the molecular weights (M_n) and polydispersities (PDI) of the obtained polymers were analyzed by size exclusion chromatography (SEC) using UV and RI detectors and calibrated by polystyrene standards (Table 1). The polymerization conditions including reaction time and concentration were carefully controlled to avoid wide disparities in the values in M_n and PDI of the copolymers. The M_n of all P3HT-Br copolymers ranged from 16 to 21 kg mol^{-1}, which should be high enough to produce highly efficient BHJ solar cells.[36,37] All P3HT-Br copolymers were found to have high regioregularity (~95%).

Four polymers, P3HT, P3HT-Br5, P3HT-Br10 and P3HT-Br20, were spun cast from chlorobenzene solutions to produce films of approximately 65 nm thick on Si substrates. The film thicknesses

Table 1. Characterization of polymers used in this study

Polymer	Br-unit 3 in feed (mol%)	Br-unit 3 in copolymer (mol%)[a]	M_n (g mol^{-1})	Polydispersity (PDI)
P3HT	0	0	16,000	1.3
P3HT-Br5	5	5.3	20,500	1.4
P3HT-Br10	10	9.1	17,400	1.3
P3HT-Br20	20	20.9	20,500	1.3

[a] Measured by ^{1}H NMR

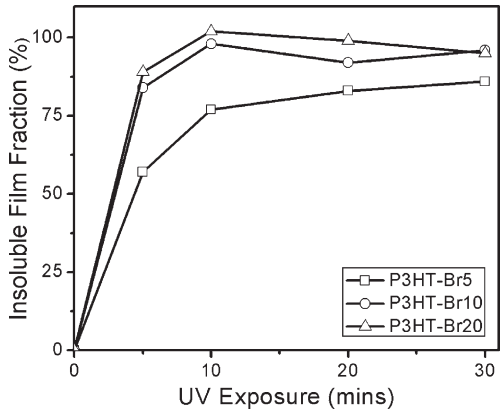

Figure 1. Photocrosslinking behavior of P3HT-Br copolymers. Insoluble film fraction as a function of UV exposure times is measured for three different P3HT-Br copolymers having 5(□), 10(○) and 20(△) mol% Br units.

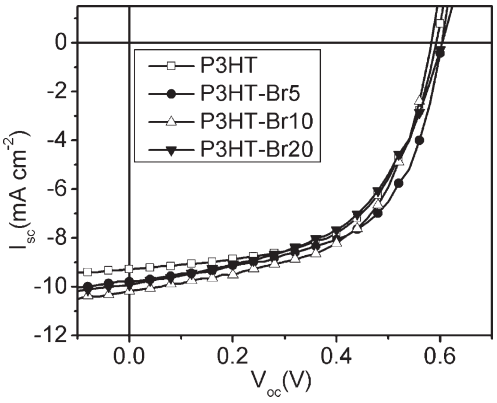

Figure 2. Current-density–voltage measurements under AM 1.5 G illumination (100 mW cm^{-2}) Four different devices of P3HT, P3HT-Br5, P3HT-Br10 and P3HT-Br20 copolymers blended with PCBM at 55:45 weight ratio showed very similar peak performances. P3HT(□): $V_{oc} = 0.59$ V, $I_{sc} = -9.27$ mA cm^{-2}, FF = 0.58, PCE = 3.16%; P3HT-Br5(●): $V_{oc} = 0.60$ V, $I_{sc} = -9.79$ mA cm^{-2}, FF = 0.57, PCE = 3.38%; P3HT-Br10(△): $V_{oc} = 0.58$ V, $I_{sc} = -10.17$ mA cm^{-2}, FF = 0.57, PCE = 3.35%; P3HT-Br20(▼): $V_{oc} = 0.60$ V, $I_{sc} = -9.92$ mA cm^{-2}, FF = 0.52, PCE = 3.11%.

were measured by surface profilometry. Figure 1 shows the photocrosslinking behavior of the P3HT-Br copolymers. P3HT did not crosslink under these conditions.

Photocrosslinking was carried out under inert argon atmosphere using UV light ($\lambda = 254$ nm) from a low power hand-held lamp (1.9 mW cm^{-2}) with exposure times ranging from 0 to 30 min. To calculate the insoluble fraction after photocrosslinking, the irradiated polymer films were immersed into chlorobenzene for 5 min, followed by rinsing with acetone for a few minutes and then dried under a stream of nitrogen. The film thicknesses before and after washing with chlorobenzene were compared. After 10 min of UV irradiation (254 nm) the films of P3HT-Br10 and P3HT-Br20 were totally insoluble whereas the pristine P3HT was not photocrosslinked at all. The trend of photocrosslinking behavior as a function of Br content is clearly evident in Figure 1. We speculate that the P3HT-Br copolymers are crosslinked via a radical mechanism initiated by the photochemical cleavage of the C-Br bonds under deep-UV irradiation at 254 nm.[38–40]

2.2. Application in Organic Photovoltaic Devices

The novel photocrosslinkable copolymers were tested both with BHJ devices to evaluate their ability to promote thermal stability, and in bilayer devices for more fundamental studies with solution cast devices.

2.2.1. Bulk Heterojunction Devices and their Thermal Stability

Figure 2 shows the current-density–voltage (I–V) characteristics of four different P3HT-Br:PCBM BHJ devices made from P3HT, P3HT-Br5, P3HT-Br10 and P3HT-Br20 copolymers, which achieved 3.16%, 3.38%, 3.35%, and 3.11% power conversion efficiency (PCE), respectively, at AM 1.5G with an intensity of 100 mW cm^{-2}. These devices were prepared under the same condition including polymer:PCBM blend ratio (55:45 by weight), solvent concentration, and post-fabrication annealing at 150 °C for 30 mins after Al electrode deposition (note that in this experiment none of the polymers have been crosslinked). It is noteworthy that all P3HT and P3HT-Br polymers show similar peak performances. While P3HT-Br5 and 10 devices show slightly higher performances than the P3HT device, P3HT-Br20 with its 20 mol% of Br-units derived from **3** shows a slight decrease in power efficiency. In addition, open circuit voltage (V_{oc}), short circuit current (I_{sc}), and fill factor (FF), which are parameters that represent device performance, show similar values for all P3HT and P3HT-Br polymers. Therefore, the incorporation of some Br substituents at the end of the hexyl side chain of P3HT does not appear to disturb the electronic properties of the copolymers or their solar cell performance.

To examine the use of photocrosslinkable P3HT-Br for enhancing the stability of BHJ devices, devices made from P3HT and P3HT-Br10 were compared and the results are shown in Figure 3. The procedure used to test the device differed from that described above because the photocrosslinking step had to be carried out before Al cathode deposition since the ITO/ glass substrate supporting BHJ film strongly absorbs the UV light at 254 nm. However, the optimized performance of BHJ devices processed by thermal annealing prior to Al electrode deposition was much lower than for the devices shown in Figure 2, as also reported by others.[10] Therefore, a solvent annealing method was used instead of the thermal annealing in order to develop the P3HT-Br:PCBM blend morphology and improve device performance.[9] Solvent annealing at 50 °C for 2–5 mins under a saturated atmosphere of chlorobenzene was therefore carried out prior to Al deposition leading to performance of 2.9% PCE for both P3HT:PCBM and P3HT-Br10:PCBM devices, a value that is somewhat lower than for the devices of Figure 2.

Figure 3 shows the thermal stability of a P3HT-Br10:PCBM BHJ device compared to that of P3HT:PCBM. Three different samples of P3HT-Br10:PCBM were prepared from the same solution. One film was used without exposure to light while the other two were exposed to UV light for 10 and 30 min, respectively, prior to Al

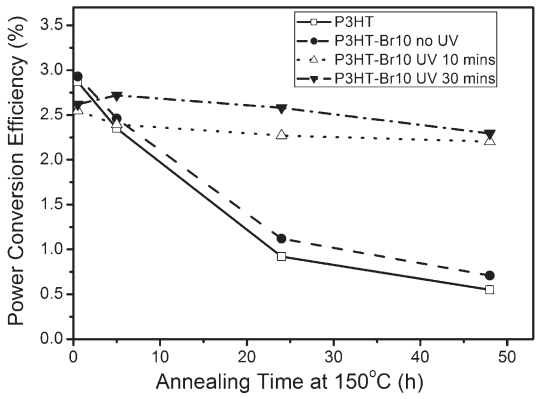

Figure 3. Efficiencies of P3HT and P3HT-Br10 devices annealed at 150 °C for different times (□: P3HT:PCBM blend; ●: P3HT-Br10:PCBM blend without UV treatment; △: P3HT-Br10:PCBM blend after being exposed to UV for 10 mins;▼: P3HT-Br10:PCBM blend after being exposed to UV for 30 mins) Four different devices were prepared under identical condition such as the ratio of polymer to PCBM and polymer concentration in chlorobenzene. The efficiency of devices without UV irradiation decreased rapidly after 5 hours of annealing, but the P3HT-Br10 devices with UV treatment show excellent thermal stability after 2 days of annealing.

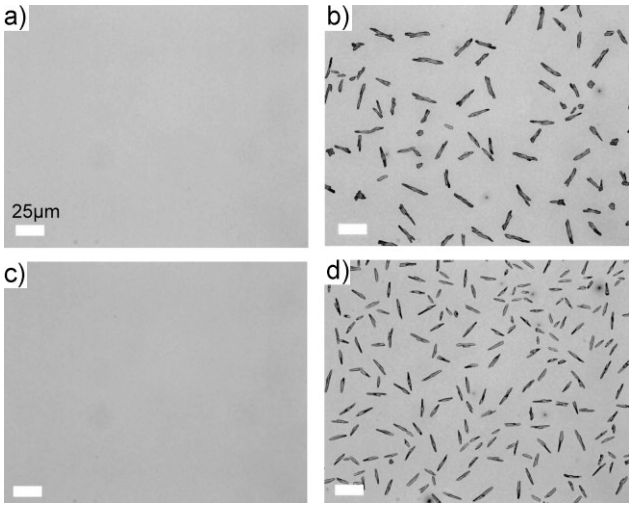

Figure 4. Optical microscopy images of P3HT-Br10:PCBM blends at 55:45 wt ratio. a) as spuncast with no thermal annealing, b) after 24 h annealing at 150 °C without exposure to UV, c) after 24 h annealing at 150 °C following exposure to UV for 30 mins. For comparison, (d) represents P3HT:PCBM blends at 55:45 wt ratio after 24 h of annealing at 150 °C. Dark areas are PCBM-rich regions. Scale bar = 25 μm.

deposition. A P3HT:PCBM blend device was also prepared without any exposure to UV light as a control experiment. After solvent annealing, both P3HT:PCBM and P3HT-Br10:PCBM devices showed similar initial performances. However, they showed a dramatic contrast in thermal stability after annealing at an elevated temperature of 150 °C, which serves as an accelerated performance test. The performance of the two different P3HT-Br10/PCBM devices treated by UV irradiation for 10 and 30 min showed very stable device performance (~90% initial device efficiency) even after 48 hr of annealing at 150 °C, which, to the best of our knowledge, represents one of the most thermally stable P3HT:PCBM BHJ devices.[21,41] In contrast, the device performance of the pristine-P3HT:PCBM blend decreased rapidly to a third of its initial efficiency value after 24 h at 150 °C. Similarly, a control sample of P3HT-Br10:PCBM without any UV treatment showed a rapid decrease in device performance at 150 °C as observed for the P3HT:PCBM blend device. This result clearly shows that the photocrosslinking concept holds promise for thermally stable high performance devices.

A deeper insight into the extreme contrast in thermal stabilities we have observed can be gleaned by examination of the active layer morphology via optical microscopy and grazing incidence wide angle X-ray scattering (GIWAXS). Optical microscopy (Leica DM 4000M) was used to provide qualitative data on the P3HT-Br:PCBM and P3HT:PCBM blend morphology. Figure 4a–c shows the optical microscopy images of P3HT-Br:PCBM (55/45) and Figure 4d shows an image for P3HT:PCBM (55/45) under a variety of conditions. These images demonstrate that thermal annealing at 150 °C induces the formation of many needle-like PCBM crystals that are over 20 μm in length in the P3HT-Br10:PCBM blend film as seen in Figure 4b, indicating that there is severe macrophase separation driven by the crystallization of the highly regioregular P3HT-Br10 polymer and PCBM molecule. In contrast, in Figure 4c the optical micrograph of the P3HT-Br10:PCBM blend crosslinked by UV treatment shows an homogeneous film free of dark PCBM crystals. These optical micrographs confirm that the photocrosslinking of P3HT-Br10 copolymers dramatically suppresses phase segregation, thus producing stable performance in solar cell devices. As a control sample, Figure 4d shows the morphology of P3HT:PCBM blends at 55:45 wt ratio after 24 h of annealing at 150 °C; again, severe phase separation of PCBM crystals is observed.

The effects of UV crosslinking on the morphology of P3HT–Br:PCBM blend as well as the crystalline structures of P3HT-Br were investigated by GIWAXS experiments. To examine the change in P3HT-Br packing structures resulting from UV crosslinking, Figure 5a and b compare the GIWAXS patterns of P3HT-Br10:PCBM blends before and after UV crosslinking. To produce surface conditions that mimic those of samples used in device measurements, a thin layer (20–30 nm) of PEDOT:PSS was spin-coated onto silicon substrates and the P3HT-Br:PCBM blend layer was spun-cast on top. Both samples were then annealed at 150 °C for 30 min, but only one sample (Figure 5b) was exposed to the UV light for 30 min and then annealed for another 30 min at 150 °C. The GIWAXS patterns of Figure 5a and b show no significant change in peak position and orientation, indicating that the packing of the polymer remains essentially undisturbed after the UV crosslinking step.

Each of the 2D image maps of GIWAXS patterns in Figure 5 can be divided into a component in the plane of the substrate (q_x) and a component perpendicular to the substrate (q_z). The (100), (200), and (300) diffraction peaks of P3HT-Br peaks are strongest in the out-of-plane direction, indicating that the P3HT-Br:PCBM blend films have a well-organized structure with planar P3HT stacks oriented along an axis perpendicular to the substrate. From the diffraction pattern in the in-plane direction (q_x), we extract a domain spacing of P3HT-Br copolymers before and after UV crosslinking. The (100), (200), and (300) peaks in P3HT-

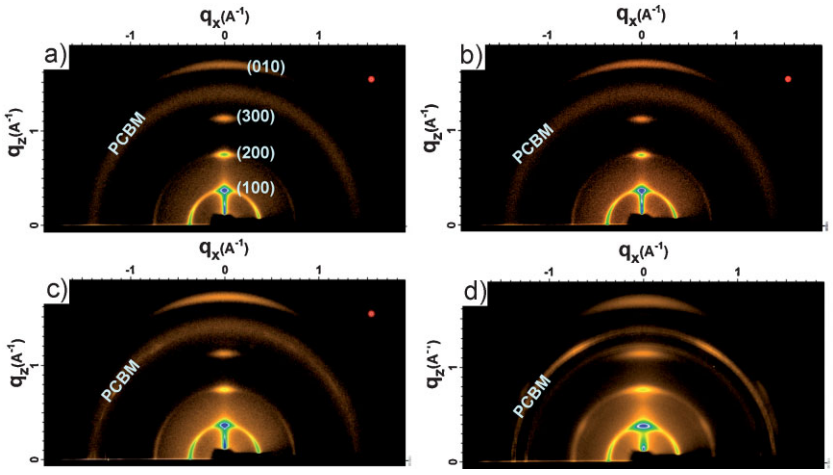

Figure 5. GIWAXS patterns of blend films of P3HT-Br10:PCBM (a–c) and P3HT:PCBM (d) at a 55:45 ratio. All samples were first annealed at 150 °C for 30 mins. a) as prepared, b) exposed to UV 30 min and then annealed for another 30 min at 150 °C, c) exposed to UV 30 min and then annealed for another 24 h at 150 °C. For comparison, (d) represents P3HT:PCBM blends at 55:45 wt ratio after 24 h of annealing at 150 °C.

Br of Figure 5a were obtained as 1.67, 0.84 and 0.55 nm, respectively, indicating that the distance between adjacent P3HT-Br alkyl chains is 1.67 nm. The peak at 0.380 nm indicates the π–π stacking distance between P3HT chains as reported elsewhere.[10,42–44] Peak positions of (100), (200) and (300) after UV crosslinking (Figure 5b) were found to be 1.69, 0.85 and 0.565 nm, respectively, indicating a slight increase by 0.2 Å in the distance between adjacent P3HT alkyl chains after UV crosslinking. This increase is most likely due to the formation of a bridged structure between alkyl chains in different P3HT lamellae, but the change is very small. In addition, the π–π stacking between P3HT-Br chains—a critical factor in charge mobility for P3HTs—is observed to be unchanged with a distance of 0.380 nm. We note that there does not appear to be any differences in π–π stacking between the P3HT-Br chains before and after UV crosslinking in these GIWAXS experiments, but high-resolution X-ray measurements are currently under investigation to examine possible quantitative differences (i.e., peak intensity).

A second set of GIWAXS patterns in Figure 5c and d compares the blend morphologies of P3HT-Br10:PCBM and P3HT:PCBM after 24 h of annealing at 150 °C to visualize the contrast in thermal stabilities. The P3HT-Br10:PCBM sample in Figure 5c was exposed to UV light for 30 min prior to 24 h annealing at 150 °C. The most distinct difference between the two treated samples comes from the crystalline peaks of PCBM at 0.46 nm spacing. While the crosslinked P3HT-Br:PCBM film in Figure 5c shows a broad PCBM peak around 0.45 nm spacing, the corresponding peak at 0.46 nm spacing for the P3HT:PCBM film of Figure 5d is both quite sharp and prominent indicating the presence of PCBM crystallites strongly phase segregated out of the P3HT/PCBM blend. This is consistent with the optical microscopy observations shown in Figure 4 and explains the large contrast in thermal stabilities between the crosslinked P3HT-Br10:PCBM and P3HT:PCBM devices.

Scheme 2 summarizes our photocrosslinking concept: after spin coating the active layer, the morphology of the BHJ is optimized by thermal annealing for a short time (i.e. 30 min at 150 °C) or by solvent annealing. Then photocrosslinking serves to freeze this optimized nanomorphology such that the device does not degrade upon further thermal annealing at elevated temperatures. On the other hand, uncrosslinked films undergo macrophase separation upon further thermal annealing and thus their performance is quickly degraded.

2.2.2. Bilayer Devices and their Thermal Stability

In order to demonstrate the advantage of photocrosslinkable P3HT-Br in bilayer devices, we have chosen the P3HT-Br/PCBM pair as a model system. Chlorobenzene was used as the solvent to produce both the P3HT-Br and the PCBM layers in sequential spin-coating operations. First, the P3HT-Br copolymers was spuncast from a 20 mg mL^{-1} chlorobenzene solution to produce a 65 nm thick film. Then, the copolymer film was crosslinked by exposure to UV light followed by annealing at 150 °C for 15 min. A thin 20 nm PCBM layer was produced by spincoating the PCBM solution in chlorobenzene on top of the crosslinked P3HT-Br layer, prior to the Al electrode deposition. Figure 6 shows the device performance of P3HT-Br5/PCBM and P3HT-Br10/PCBM bilayer devices.

I–V characteristics of optimized P3HT-Br5/PCBM and P3HT-Br10/PCBM bilayer devices under standard illumination conditions at 100 mW cm^{-2} are shown in Figure 6a while device characteristics are summarized in Table 2. Both of the bilayer devices P3HT-Br5/PCBM and P3HT-Br10/PCBM afforded high efficiency values (PCE) of 2.1% and 2.2%; these values represent some of the highest performance ever achieved for bilayer devices fabricated by solution processing. Such high performance is likely related to the minimal disturbance in the π–π stacking of the judiciously designed P3HT-Br copolymer upon crosslinking, as demonstrated by the GIWAXS study shown in Figure 5. It is also interesting to note that the open circuit voltage of the devices is

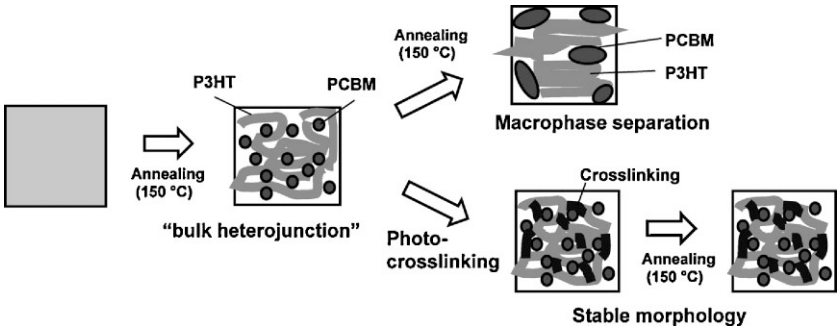

Scheme 2. Schematic representation of the photocrosslinking approach used in this study.

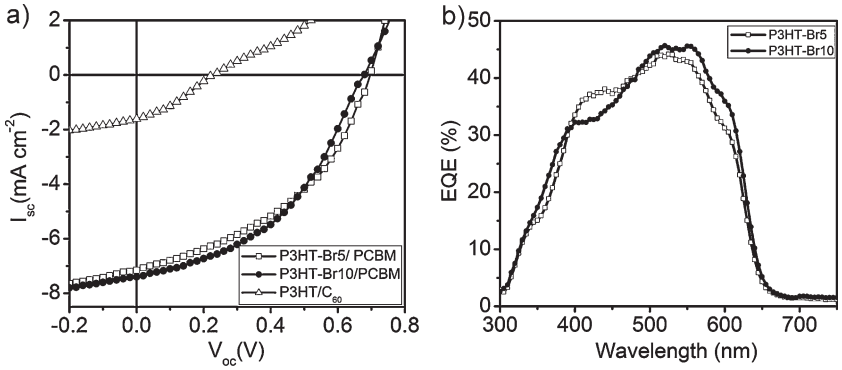

Figure 6. a) Current density-voltage curves of optimized P3HT-Br5/PCBM (□), P3HT-Br10/PCBM (●) bilayer devices, and a P3HT/C_{60} (△) bilayer with the same thickness. b) Spectral response of P3HT-Br5/PCBM (□) and P3HT-Br10/PCBM (●) bilayer devices.

0.7 V, which is 0.1 V higher than that of the BHJ devices. This may be due to the better wetting of the bottom electrode by P3HT-Br and the top electrode by PCBM in the bilayer device than is the case for the BHJ device in which P3HT and PCBM are mixed within the bulk.[18,45,46]

To investigate the spectral response of P3HT-Br/PCBM bilayers at a given wavelength, the external quantum efficiency (EQE) was measured for two optimized P3HT-Br5/PCBM and P3HT-Br10/PCBM devices as shown in Figure 6b. EQE values for both devices are higher than 40% around the absorption peak of the polymer at $\lambda = 550$ nm.

To further clarify the advantage of using crosslinkable P3HT-Br in a bilayer device, a P3HT/C_{60} bilayer device was produced by vapor deposition of C_{60} for comparison. The film thicknesses of P3HT and C_{60} layers were kept as 65 nm and 20 nm, respectively, thus allowing a comparison with the solution processed P3HT-Br/PCBM bilayer devices having the same thicknesses as used in Figure 6a. It was found that the power efficiency of the vapor deposited P3HT/C_{60} bilayer device remained very low (0.12%). This remarkable contrast in device performances clearly demonstrates the usefulness of P3HT-Br copolymers for use in multilayer solar cells.

As seen in Figure 7 the thermal stability of the UV-crosslinked P3HT-Br10/PCBM bilayer devices is excellent. This is in sharp contrast with the performance of a bulk heterojunction P3HT/PCBM device subjected to the same thermal treatment at 150 °C for which morphology development with phase separation degrades device performance.

To gain further insight into the workings of bilayer devices, the effect of active layer thicknesses on device performance was investigated, as shown in Figure 8. Two different series of samples were produced under identical conditions as described above but the polymer solution concentration was varied. In a first set of experiments, the thickness of the PCBM layer was systematically varied from 10 nm to 60 nm, while the thickness of P3HT-Br was fixed at 65 nm (Figure 8a). A second set of devices was made with a constant PCBM film thickness of 25 nm while the P3HT-Br layer thickness was varied from 15 nm to 95 nm (Figure 8b). The results shown in Figure 8 show a clear dependence of device performance on active layer thicknesses. For example, the efficiency of the bilayer device increases dramatically from 0.85% to 2.13% as the PCBM film thickness is increased from 10 to 20 nm. However, as the PCBM layer thickness is increased up to 60 nm, the device performance decreases to 0.42%. The data shown in Figure 8 for the two sets of devices suggests that best bilayer device performance is obtained for layer thicknesses of 65 nm and 20 nm for the P3HT-Br and PCBM layers, respectively. As expected, the optimized bilayer device requires a relatively thick film for the electron donating P3HT-Br layer since it is almost solely responsible for the absorption of light. However, since the layer thickness is limited by the finite length of exciton diffusion as well as by charge transport, the P3HT film thickness should be optimized to balance these factors. On the other hand, due to its very small contribution to light absorption, a thinner PCBM layer is better for charge transport since it reduces the pathway to the electrode. In spite of this, we believe that the optimum PCBM layer thickness is 20–25 nm as the PCBM layer itself can help maximize the light intensity within the P3HT layer near the interface where most of effective excitons are generated. This is because the light intensity near the metallic electrode is expected to be low due to optical interference effect.[4,47] In addition, it is difficult to produce the uniform thin films, which are

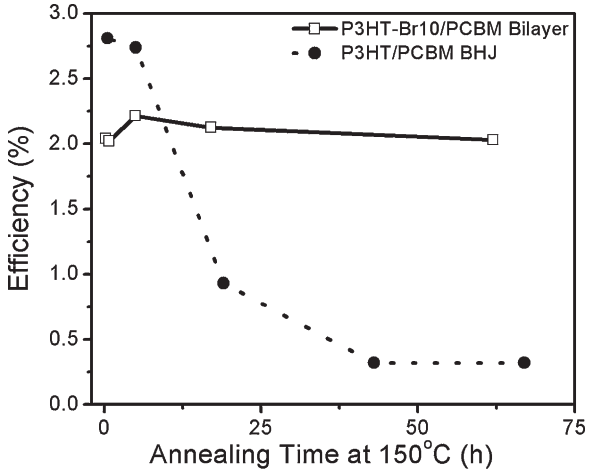

Figure 7. Efficiency of UV crosslinked P3HT-Br10/PCBM bilayer devices as a function of annealing time at 150 °C (□). The efficiency of P3HT/PCBM BHJ devices subjected to the same annealing conditions at 150 °C (●) is shown for comparison purposes. The efficiency of the uncrosslinked P3HT BHJ devices decreased drastically after 17 h annealing, while the UV crosslinked bilayer P3HT-Br10 devices show excellent long-term thermal stability.

Table 2. Bilayer device performances of P3HT-Br/PCBM and P3HT/C_{60}

Device	V_{oc} (V)	J_{sc} (mA cm^{-2})	Fill Factor	PCE (%)
P3HT/C_{60}	0.23	−1.61	0.32	0.12%
P3HT-Br5/PCBM	0.70	−7.15	0.43	2.13%
P3HT-Br10/PCBM	0.68	−7.40	0.44	2.22%

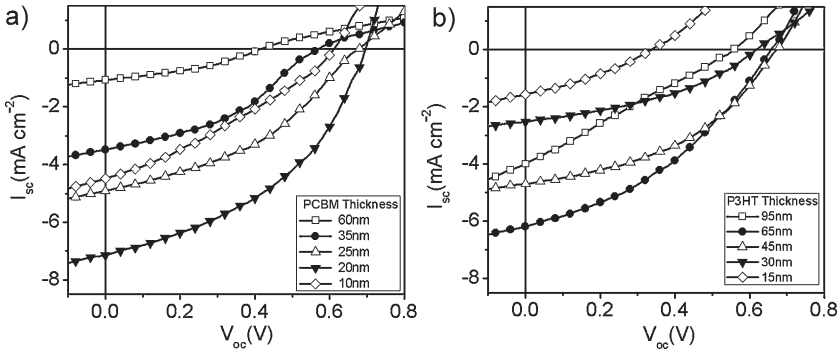

Figure 8. P3HT-Br5/PCBM bilayer device performance as a function of film thicknesses of PCBM (a) and P3HT-Br5 (b).

required for a good contact between the PCBM layer and the cathode when the thickness is $\leq$10 nm.

The topology of the interface between P3HT-Br and PCBM layers was examined by atomic force microscopy (AFM). This interfacial topology is a critical factor for bilayer device performance as the diffused interface between electron donor and acceptor is beneficial to bilayer devices by increasing the effective area for electron–hole dissociation.[27,48,49] In order to investigate the interface of the donor/acceptor layers, P3HT-Br10 copolymers were spuncast from chlorobenzene to produce two different films having the same 65 nm thickness. Both samples were exposed to UV light for 30 min and then annealed for 15 min at 150 °C, as was done in the preparation of bilayer devices. For one of the samples, a PCBM layer was spuncast on top of the P3HT-Br layer. Subsequently, the PCBM layer was carefully removed by soaking the sample into chlorobenzene for 20 min, followed by careful rinsing. A comparison of the AFM images of the two P3HT-Br layers was then carried out (Fig. 9). First, it should be noted that the film thicknesses of two different samples remained the same at 65 nm, indicating that both films were crosslinked and insoluble; in addition, the surface roughness obtained from the height images of the two different samples (Fig. 9a and c) also did not change at about 4 nm. The phase images in Figure 9b and d also suggest the same qualitative interfacial topology for both samples. Therefore, these observations suggest that bilayer structure

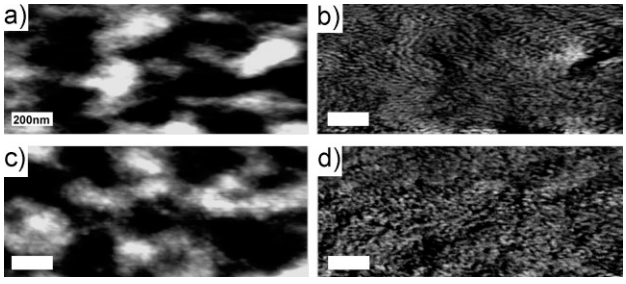

Figure 9. AFM images showing the surface topology of P3HT-Br10. Height image (a) and phase image (b) of crosslinked P3HT-Br10 film. Height image (c) and phase image (d) of crosslinked P3HT-Br10 film after removal of the PCBM layer. RMS roughness: a) 4.6 nm, c) 3.8 nm. The film thicknesses of P3HT-Br10 layer (65 nm) remain unchanged.

obtained from photocrosslinked P3HT-Br and subsequent spin-coating of PCBM from the same solvent has a planar interface with relatively small degree of roughness, and no significant penetration of PCBM molecules into the P3HT-Br layer is found. We therefore believe that further effort targeting engineering of the interface might be beneficial to further enhance device performance as a slightly less well-defined interface would likely be beneficial.

3. Conclusions

It is clear from this work that the new crosslinkable monomer **3** we have developed is of value in the preparation of efficient polymer based organic solar cells. The light sensitive unit attached at the end of the hexyl chain of P3HT does not appear to disturb the π–π stacking of the polythiophene backbone. A clear advantage of the photocrosslinking strategy is that crosslinking can be decoupled from thermal annealing, a valuable feature for BHJ solar cells that require some annealing to achieve optimum nanomorphology before crosslinking is used in order to freeze this optimum morphology and preserve long term performance. As a result, BHJ solar cells based on P3HT-Br:PCBM show remarkably enhanced thermal stability when compared to conventional devices utilizing a P3HT:PCBM blend. This dramatic contrast in thermal stabilities was clearly visualized by optical microscopy as well as GIWAXS. No PCBM crystallite is found in the crosslinked P3HT-Br:PCBM blend film even after 24 h of annealing at 150 °C. In contrast, many micrometer-size crystallites are present in the non-crosslinked P3HT-Br:PCBM film. In addition, GIWAXS reveals that incorporating Br units into the polymer has little effect on the polythiophene packing. The photocrosslinkable P3HT-Br shines in its performance for solution processed bilayer devices, in which PCBM is deposited on the top of crosslinked P3HT-Br films using the same solvent. Remarkably efficient bilayer devices with 2.2% power efficiency and excellent thermal stability have been obtained. Because of the ability to crosslink one of the layers making it impervious to subsequent processing steps, devices with the bilayer architecture can also be used as a convenient platform to study the intrinsic performance of new materials, as well as exciton dynamics, charge separation, and charge transport. This work establishes some of the fundamental rules needed for the design of crosslinkable materials that may be used broadly with other photovoltaic systems.

4. Experimental

Materials: Unless otherwise noted, all reagents were used as received and without further purification, or were prepared according to literature procedures. Chromatography was carried out with silica gel for flash columns, 230–400 mesh. Unless otherwise specified, extracts were dried over $MgSO_4$ and solvents were removed with a rotary evaporator under reduced pressure. All NMR spectra were measured in $CDCl_3$ with TMS or solvent signals as the standards. 2-Bromo-3-hexylthiophene was purchased from ALDRICH.

Synthesis of 2-bromo-3-(6-bromohexyl) thiophene: 3-bromothiophene (10.2 g, 0.0626 mol) was dissolved in dried hexane (80 mL), and the solution was cooled to −78 °C. 25 ML of 2.5 M n-BuLi hexane solution was then added dropwise, and the solution was stirred at this temperature for 10 min. Dry THF (7 mL) was then added dropwise until the white 3-lithiothiophene salt precipitated. The solution was then stirred for 1 h, then allowed to warm to −10 °C. Dry THF (3 mL) and 1,6-dibromohexane (37 mL, 0.24 mol) were then added to the solution. The solution was stirred at room temperature (RT) for 2 h, then washed with water (3 × 300 mL). The organic layer was dried over anhydrous $MgSO_4$, filtered and concentrated. Distillation at 60 °C at 0.18 mbar gave a light-yellow oil, which was purified via silica gel column chromatography using hexane as the eluent. 3-(6-Bromohexyl) thiophene **(2)** was obtained as a colorless oil (4.33g, 28.0% yield). ^{1}H-NMR (500 MHz, $CDCl_3$) δ(ppm): 7.23 (dd, J = 7.85, 2.95, 1H), 6.92–6.94 (m, 2H), 3.40 (t, J = 6.8, 2H), 2.63 (t, J = 7.6, 2H), 1.83–1.89 (m, 2H), 1.61–1.67 (m, 2H), 1.44–1.50 (m, 2H), 1.33–1.39 (m, 2H). ^{13}C-NMR (500 MHz, $CDCl_3$) δ(ppm): 142.74, 128.10, 125.07, 119.81, 33.89, 32.61, 30.22, 30.01, 28.28, 27.87. MS: m/z calcd 248.0057; found 248.0054.

3-(6-Bromohexyl) thiophene (4.33 g, 0.0175 mol) was dissolved in dry THF (60 mL). The solution was cooled in an ice bath, and 1,3-dibromo-5,5-dimethylhydantoin (2.63 g, 0.00919 mol) was added and the mixture was stirred at RT for 2 hrs. After concentrating the mixture under reduced pressure dry hexane was added, and the mixture was filtered and concentrated. Further purification was carried out via silica gel column chromatography, using hexane as the eluent. The resulting product was dried under vacuum to yield 2-bromo-3-(6-bromohexyl) thiophene **(3)** as a light-yellow oil (4.33 g, 76% yield). ^{1}H-NMR (500 MHz, $CDCl_3$,) δ(ppm): 7.18 (d, J = 5.6, 1H), 6.78 (d, J = 5.6, 1H), 3.39 (t, J = 6.8, 2H), 2.56 (t, J = 7.6, 2H), 1.84–1.90 (m, 2H), 1.55–1.62 (m, 2H), 1.44–1.50 (m, 2H), 1.32–1.38 (m, 2H). ^{13}C-NMR (500 MHz, $CDCl_3$,) δ(ppm): 141.54, 128.12, 125.24, 108.90, 33.91, 32.65, 29.46, 29.16, 28.21, 27.88. MS: m/z calcd 325.9162; found 325.9168. CHS anal. calcd for $C_{10}H_{14}Br_2S$: C 36.83, H 4.33, S 9.83. Found: C 36.62, H 4.26, S 9.44.

Preparation of the P3HT-Br10 Copolymer: Lithium diisopropylamide (LDA) was generated by addition of n-BuLi (2.5 M in hexane, 3.0 mL, 7.50 mmol) to a solution of dry diisopropylamine (1.35 mL, 9.55 mmol) in dry THF (18 mL) at −78 °C. The solution was stirred at this temperature for 1 h. The freshly generated LDA solution was added dropwise to the mixture of 2-bromo-3-(6-bromohexyl)thiophene **(3)** (0.262 g, 0.804 mmol) and 2-bromo-3-hexylthiophene **(4)** (1.79 g, 7.24 mmol) in dry THF (75 mL) at −78 °C. After 1 h reaction at −78 °C, anhydrous $ZnCl_2$ (1.29 g, 9.46 mmol) was added portionwise to the mixture, which was stirred for 30 mins and then warmed slowly to RT. Polymerization initiated by addition of $Ni(dppp)Cl_2$ (0.0525 g, 0.097 mmol) to the mixture was carried out at RT for 45 mins. The solution was quenched by 1.5 mL of 1.0 N aqueous HCl in order to stop the polymerization. The polymer was precipitated with MeOH (450 mL) containing 4.5 mL of NH_3 7N in MeOH solution to neutralize it, and the resulting precipitate was then filtered. Oligomers and impurities in the product were removed by Soxhlet extractions with MeOH for > 3 h, followed by hexane extraction for > 5 h. The resulting solid was dried under vacuum to yield the product (**5**). ^{1}H-NMR (500 MHz, $CDCl_3$) δ(ppm): 6.96 (s, ArH), 3.40 (br t, Br-CH_2), 2.78 (br t, Ar-CH_2), 1.87 (br m, BrCH_2−CH_2), 1.69 (br m, CH_3CH_2−CH_2), 1.2-1.5 (br m, CH_2), 0.89 (s, CH_3) ^{13}C-NMR (500 MHz, $CDCl_3$) δ(ppm): 139.86, 133.66, 130.45, 128.56, 33.88, 32.71, 31.69, 30.50, 30.29, 29.45, 29.26, 28.61, 27.98, 22.65, 14.13.

AFM Measurements: A Multimode AFM (Veeco Instruments) was used in a tapping mode to investigate the two-dimensional surface topology of crosslinked P3HT-Br10 films. Two different P3HT-Br10 films were spuncast from 20 mg mL^{-1} chlorobenzene solution on PEDOT as used for the device fabrication. Both samples were crosslinked by exposing them to UV for 30 min and then were annealed at 150 °C for 15 min. PCBM solution in 15 mg mL^{-1} chlorobenzene was spuncast on the second sample only for a comparison test. The PCBM layer was then removed by soaking the sample into chlorobenzene for 20 min and rinsing it several times with the same solvent.

GIWAXS Measurements: For GISAXS measurements, to produce identical surface conditions as samples for device measurement, a thin layer (20–30 nm) of PEDOT:PSS was spun onto silicon substrates and the P3HT-Br10:PCBM or P3HT:PCBM blend layer was then spin-coated on top. GISAXS measurements were performed on beamline 11.3 in the Stanford Synchrotron Radiation Laboratory. X-rays with a wavelength of 0.9752 Å were used. The incidence angle (∼0.1°) was carefully chosen to allow for complete X-ray penetration into the polymer film. The scattering spectra were collected as the 2D image map that can be divided into a component in the plane of the substrate (q_x) and a component perpendicular to the substrate (q_z).

Devices Fabrication and Measurement: ITO-coated glass substrates were subjected to ultrasonication in different solvent systems including acetone, 2% soap in water, deionized water, and then 2-propanol. Each step was carried out for 20 min. The substrates were then dried under a stream of nitrogen. A filtered dispersion of PEDOT:PSS in water (Baytron-PH500) was spuncast at 3 400 RPM for 60 s to produce a 25 nm thick layer, followed by baking for 10 min at 140 °C. All procedures after this point were performed in an inert-atmosphere (Ar) glove box. Two different solutions of P3HT-Br and PCBM in chlorobenzene (30 mg mL^{-1}) were prepared separately and the P3HT-Br solution was stirred at 110 °C for more than 24 h to ensure complete dissolution. The solutions were passed through a 0.45 μm polytetrafluoroethylene syringe filter, prior to use in the device.

For P3HT-Br:PCBM BHJ device, the P3HT-Br:PCBM blend solution (55:45 by weight) was prepared with the polymer concentration of ∼14 mg mL^{-1} and was stirred at RT overnight. The blend solution was applied to the substrate and spun at 1200 RPM for 60 s. The solvent annealing was performed under saturated atmosphere of chlorobenzene at 50 °C within a covered Petri dish for 2–5 minutes. Then, the polymer films were irradiated at 254 nm with a hand held UV lamp (typically used for visualization in thin layer chromatography, UV light intensity: ca. 1.9 mW cm^{-2}). For P3HT-Br/PCBM bilayer device, the P3HT-Br solution was applied to the substrate and spun at 2000 RPM for 60 s. The spuncast P3HT-Br films were irradiated at 254 nm with a hand held UV lamp (UV light intensity: ca. 1.9 mW cm^{-2}) and annealed at 150 °C for 15 min. Finally, the PCBM solution was spuncast at 2000 RPM for 60 s on the top of the photocrosslinked P3HT-Br film.

A 100 nm thick Al cathode was deposited by thermal evaporation under vacuum (10^{-6} torr). A part of the organic layer was removed to allow contact with the ITO, and then conductive Ag paste was painted to the area in order to produce the electrical contact. Annealing was performed after Al deposition using a temperature-controlled hot plate at 150 °C. All devices were measured at RT under an argon atmosphere with an Oriel xenon arc lamp equipped with an AM 1.5G solar filter. Current–voltage behavior was recorded with a Keithly 236 SMU. The active area was 0.03 cm^2.

Acknowledgements

B. J. K and Y. M. contributed equally to this work. Financial support of this work by the Office of Science, Office of Basic Energy Sciences, of the U.S. Department of Energy under Contract No. DE-AC0205CH11231. A portion of the work was performed at the Molecular Foundry and the Stanford Synchrotron Radiation Laboratory also supported by the US Department of Energy. Y.M. thanks JSR Corporation for support. The authors acknowledge Dr. M. F. Toney at SSRL for assistance in GIWAXS measurements

Received: January 10, 2009
Revised: March 29, 2009
Published online: May 22, 2009

[1] T. L. Benanti, D. Venkataraman, *Photosynth. Res.* **2006**, *87*, 73.
[2] K. M. Coakley, M. D. McGehee, *Chem. Mater.* **2004**, *16*, 4533.
[3] S. Gunes, H. Neugebauer, N. S. Sariciftci, *Chem. Rev.* **2007**, *107*, 1324.
[4] H. Hoppe, N. S. Sariciftci, *J. Mater. Res.* **2004**, *19*, 1924.
[5] B. C. Thompson, J. M. J. Fréchet, *Angew. Chem. Int. Ed.* **2008**, *47*, 58.
[6] J. J. M. Halls, C. A. Walsh, N. C. Greenham, E. A. Marseglia, R. H. Friend, S. C. Moratti, A. B. Holmes, *Nature* **1995**, *376*, 498.
[7] G. Yu, J. Gao, J. C. Hummelen, F. Wudl, A. J. Heeger, *Science* **1995**, *270*, 1789.

[8] S. E. Shaheen, C. J. Brabec, N. S. Sariciftci, F. Padinger, T. Fromherz, J. C. Hummelen, *Appl. Phys. Lett.* **2001**, *78*, 841.
[9] G. Li, V. Shrotriya, J. S. Huang, Y. Yao, T. Moriarty, K. Emery, Y. Yang, *Nat. Mater.* **2005**, *4*, 864.
[10] W. L. Ma, C. Y. Yang, X. Gong, K. Lee, A. J. Heeger, *Adv. Funct. Mater.* **2005**, *15*, 1617.
[11] J. K. Lee, W. L. Ma, C. J. Brabec, J. Yuen, J. S. Moon, J. Y. Kim, K. Lee, G. C. Bazan, A. J. Heeger, *J. Am. Chem. Soc.* **2008**, *130*, 3619.
[12] M. M. Wienk, M. Turbiez, J. Gilot, R. A. J. Janssen, *Adv. Mater.* **2008**, *20*, 2556.
[13] C. P. Chen, S. H. Chan, T. C. Chao, C. Ting, B. T. Ko, *J. Am. Chem. Soc.* **2008**, *130*, 12828.
[14] S. A. Backer, K. Sivula, D. F. Kavulak, J. M. J. Fréchet, *Chem. Mater.* **2007**, *19*, 2927.
[15] J. Y. Kim, K. Lee, N. E. Coates, D. Moses, T. Q. Nguyen, M. Dante, A. J. Heeger, *Science* **2007**, *317*, 222.
[16] M. Reyes-Reyes, K. Kim, D. L. Carroll, *Appl. Phys. Lett.* **2005**, *87*, 083506.
[17] W. L. Ma, A. Gopinathan, A. J. Heeger, *Adv. Mater.* **2007**, *19*, 3656.
[18] X. N. Yang, J. Loos, S. C. Veenstra, W. J. H. Verhees, M. M. Wienk, J. M. Kroon, M. A. J. Michels, R. A. J. Janssen, *Nano Letters* **2005**, *5*, 579.
[19] D. E. Markov, E. Amsterdam, P. W. M. Blom, A. B. Sieval, J. C. Hummelen, *J. Phys. Chem. A* **2005**, *109*, 5266.
[20] S. R. Scully, M. D. McGehee, *J. Appl. Phys.* **2006**, *100*, 034907.
[21] K. Sivula, Z. T. Ball, N. Watanabe, J. M. J. Fréchet, *Adv. Mater.* **2006**, *18*, 206.
[22] M. Drees, H. Hoppe, C. Winder, H. Neugebauer, N. S. Sariciftci, W. Schwinger, F. Schaffler, C. Topf, M. C. Scharber, Z. G. Zhu, R. Gaudiana, *J. Mater. Chem.* **2005**, *15*, 5158.
[23] Z. Zhu, S. Hadjikyriacou, D. Waller, R. Gaudiana, *J. Macromol. Sci., Part A: Pure Appl. Chem.* **2004**, *41*, 1467.
[24] E. J. Zhou, Z. Tan, C. H. Yang, Y. F. Li, *Macromol. Rapid Commun.* **2006**, *27*, 793.
[25] M. M. Alam, S. A. Jenekhe, *Chem. Mater.* **2004**, *16*, 4647.
[26] H. Gommans, D. Cheyns, T. Aernouts, C. Girotto, J. Poortmans, P. Heremans, *Adv. Funct. Mater.* **2007**, *17*, 2653.
[27] J. G. Xue, S. Uchida, B. P. Rand, S. R. Forrest, *Appl. Phys. Lett.* **2004**, *84*, 3013.
[28] P. Peumans, A. Yakimov, S. R. Forrest, *J. Appl. Phys.* **2003**, *93*, 3693.
[29] K. Schulze, C. Uhrich, R. Schuppel, K. Leo, M. Pfeiffer, E. Brier, E. Reinold, P. Bauerle, *Adv. Mater.* **2006**, *18*, 2872.
[30] Y. Shirota, H. Kageyama, *Chem. Rev.* **2007**, *107*, 953.
[31] H. J. Snaith, N. C. Greenham, R. H. Friend, *Adv. Mater.* **2004**, *16*, 1640.
[32] L. H. Nguyen, H. Hoppe, T. Erb, S. Gunes, G. Gobsch, N. S. Sariciftci, *Adv. Funct. Mater.* **2007**, *17*, 1071.
[33] Y. Kim, S. Cook, K. J, J. Nelson, J. R. Durrant, D. D. C. Bradley, M. Giles, M. Heeney, R. Hamilton, I. McCulloch, *J. Phys. Chem. C* **2007**, *111*, 8137.
[34] K. K. Stokes, K. Heuze, R. D. McCullough, *Macromolecules* **2003**, *36*, 7114.
[35] J. S. Liu, R. D. McCullough, *Macromolecules* **2002**, *35*, 9882.
[36] R. C. Hiorns, R. De Bettignies, J. Leroy, S. Bailly, M. Firon, C. Sentein, A. Khoukh, H. Preud'homme, C. Dagron-Lartigau, *Adv. Funct. Mater.* **2006**, *16*, 2263.
[37] A. M. Ballantyne, L. Chen, J. Dane, T. Hammant, F. M. Braun, M. Heeney, W. Duffy, I. McCulloch, D. D. C. Bradley, J. Nelson, *Adv. Funct. l Mater.* **2008**, *18*, 2373.
[38] K. S. Lee, K. Y. Yeon, K. H. Jung, S. K. Kim, *J. Phys. Chem. A* **2008**, *112*, 9312.
[39] Y. R. Lee, C. C. Chen, S. M. Lin, *J. Chem. Phys.* **2003**, *118*, 10494.
[40] Y. Tang, L. Ji, R. S. Zhu, Z. R. Wei, B. Zhang, *J. Phys. Chem. A* **2005**, *109*, 11123.
[41] K. Sivula, C. K. Luscombe, B. C. Thompson, J. M. J. Fréchet, *J. Am. Chem. Soc.* **2006**, *128*, 13988.
[42] T. Erb, U. Zhokhavets, G. Gobsch, S. Raleva, B. Stuhn, P. Schilinsky, C. Waldauf, C. J. Brabec, *Adv. Funct. Mater.* **2005**, *15*, 1193.
[43] R. J. Kline, M. D. McGehee, E. N. Kadnikova, J. S. Liu, J. M. J. Fréchet, M. F. Toney, *Macromolecules* **2005**, *38*, 3312.
[44] R. D. Mccullough, S. Tristramnagle, S. P. Williams, R. D. Lowe, M. Jayaraman, *J. Am. Chem. Soc.* **1993**, *115*, 4910.
[45] W. L. Ma, C. Y. Yang, A. J. Heeger, *Adv. Mater.* **2007**, *19*, 1387.
[46] X. Yang, J. Loos, *Macromolecules* **2007**, *40*, 1353.
[47] L. A. A. Pettersson, L. S. Roman, O. Inganas, *J. Appl. Phys.* **1999**, *86*, 487.
[48] M. Drees, K. Premaratne, W. Graupner, J. R. Heflin, R. M. Davis, D. Marciu, M. Miller, *Appl. Phys. Lett.* **2002**, *81*, 4607.
[49] E. L. Ratcliff, J. L. Jenkins, K. Nebesny, N. R. Armstrong, *Chem. Mater.* **2008**, *20*, 5796.